Segregation of Phosphorus and Sulfur in Heat-Affected Zone Hot Cracking of Type 308 Stainless Steel

Through the use of Auger analysis, sulfur is characterized as having a greater effect on heat-affected zone cracking than phosphorous

BY L. LI AND R. W. MESSLER, JR.

ABSTRACT. The Auger mieroprobe analysis method was employed to identify the presence and characterize the degree of interfacial segregation of P and S associated with weld heat-affected zone hot cracking in Type 308 austenitic stainless steel. Crack surfaee samples for Auger analysis were produced under a controlled evacuated and argon back-filled atmosphere on a Gleeble™ thermomechanical simulator. Sulfur was found to strongly segregate to the intergranular fracture surface, while segregation of P, confirmed by earlier EDS analysis, was undetected by the Auger equipment employed. The relatively stronger tendency for S to segregate correlates well with this element's higher diffusion rate compared to P and with eracking suseeptibility test results (Ref. 1), which showed S to be more detrimental than P to HAZ cracking.

Introduction

In a recent study to differentiate the normally combined effects of phosphorus (P) and sulfur (S) on the weld hot-eracking susceptibility of austenitic stainless steels, five heats of Type 308 were custom designed and melted with a combined P+S level of 0.032 wt-%, representing very low S and high P, very low P and high S, and equal amounts of each (Ref. 1). The effects of various individual P and S levels on weld hot-cracking behavior were studied using the Varestraint test and hot ductility tests. Phosphorus and sulfur partitioning and observed effects on weld penetration and solidificaation substructure were studied using optical and scanning electron microscopy and quantitative electron microprobe. It was shown P is more potent in exacerbating hot-cracking susceptibility in the fusion zone, and S is more potent in exacerbating hot cracking in the heat-affected zone.

The observed stronger effect of P in weld-fusion-zone cracking is not new. For example, Brooks (Ref. 2) observed a more detrimental effect of P than S on solidificaation hot cracking in austenitic stainless steels. In a series of studies, Arata, *et al.* (Refs. 3, 4), also found P to have a much greater influence in deteriorating solidification cracking resistance than S. It was suggested the detrimental effect of P was due to its segregation to interdendritic regions and the subsequent formation of low-melting phosphides. The less detrimental effect of S on solidification cracking was believed to be due to the S being tied up in diserete and seemingly benign MnS particles.

The observed greater detrimental effect of S in the heat-affected-zone hot cracking of austenitic stainless steels has not, to our knowledge, been reported before. Although the segregation of P and S during isothermal heat treatment has been recently studied (Ref. 5), no differentiation between the individual roles of P and S was established. Furthermore, there has not been a systematic study of the segregation and redistribution of P and S in the weld HAZ of austenitic stainless steels, particularly with respect to the potentially different roles P and S may play. The study reported here presents a preliminary attempt to investigate this problem.

KEY WORDS

Auger Analysis
Heat-Affected Zone (HAZ)
Hot Cracking
Stainless Steel
Phosphorus
Sulfur
P and S Segregation

Experimental Procedure

Crack surfaces for microfissures in the HAZ, whether from an actual weld joint or from Varestraint tested samples, are not readily extractable by Auger analysis because such microfissures are typically on the order of 0.1 mm in length. Even if the microfissures were successfully extracted, the oxidation of the crack surface that occurs as a weld cools has prevented effective Auger examination of elements present. Therefore, in this study, crack surfaces of microfissures from the HAZ were simulated under controlled atmosphere by using a Model 3500 Gleeble™ thermomechanical simulator.

Gleeble simulation procedures employed in this study involved testing samples from two heats of test materials (Table 1) with a constant combined P and S of 0.032 wt-%, but with high P-low S (HP/LS) and low P-high S (LP/HS). Test specimens were 102-mm-long round bars, 6.4 mm in diameter. The thermal cycles were calculated for 38-mm-thick stainless steel, shielded metal arc welded with 2.8-kJ/mm heat input and a 22°C initial temperature. Thermal cycles with various peak temperatures were generated using the f(s,d) method on the Gleeble (Ref. 6). During testing, the following techniques and procedures were used: 1) A separate wire thermocouple technique was employed for temperature acquisition and control; 2) Gleeble jaw separation was 20 mm; 3) Gleeble crosshead speed for pulling specimen was 63.5 mm/s; 4) the hold time at the test temperature was 0; 5) multiple samples were employed for each test condition; 6) after the sample was secured in the Gleeble jaws, the test chamber was twice evacu-

L. LI (leijun.li@uni.edu) *is Assistant Professor in the Industrial Technology Department at the University of Northern Iowa, Cedar Falls, Iowa. R. W. MESSLER, JR., is Professor in the Materials Science and Engineering Department at Rensselaer Polytechnic Institute in Troy, N.Y.*

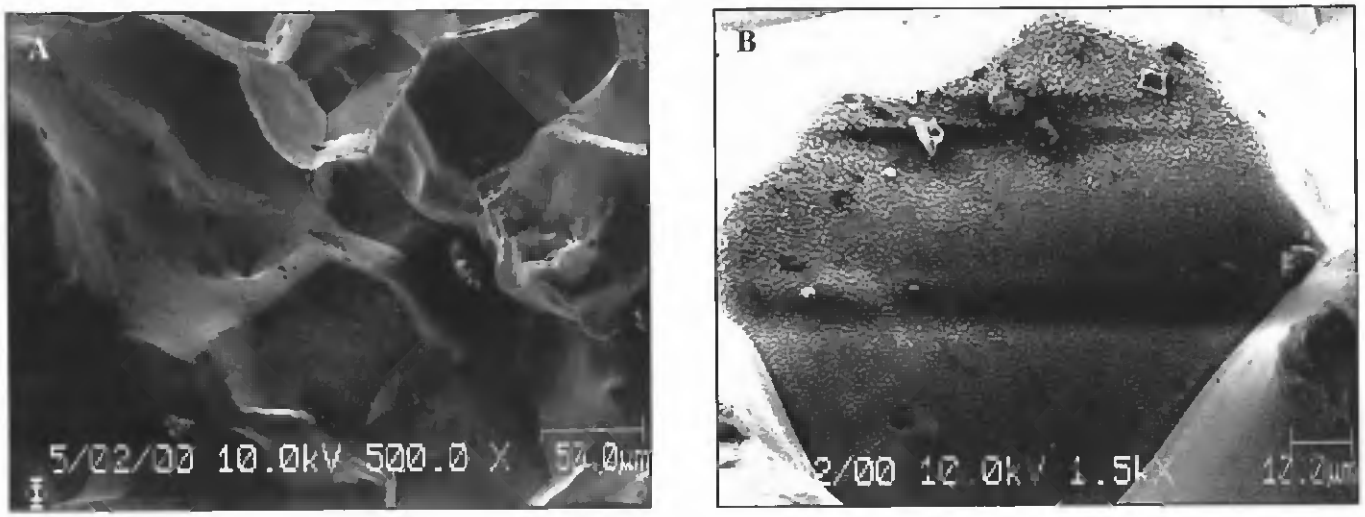

Fig. 1 — The secondary electron images for fractured surfaces of HAZ cracks formed at the zero-ductility temperature for Heat LP/HS. A — 500X; B — 1500X.

ated to 1 x 10^{-3} torr and backfilled with argon before testing; 7) the zero ductility temperature (ZDT) upon heating, at which the ductility of the test material drops to zero, was found by systematically varying the peak temperature of the thermal cycle. Crack surface samples were extracted from Gleeble coupons tested at the ZDT temperatures by manually cutting with a hacksaw. A cutting fluid was used, and extracted samples were ultrasonically cleaned in water and dried. No further treatment was done on the samples prior to Auger analysis.

The extracted crack samples were analyzed on a PHI 680 Field Emission Scanning Auger Nanoprobe with the following test procedures. The Auger analysis started by obtaining the surface morphology in the instrument's secondary electron-image mode. Once an area of interest was identified, Auger survey scans were collected from different points in the imaged area to detect elements present on the crack surface. From these data, a mapping of detected elements was obtained. The Auger analysis beam was produced with 10 kV acceleration voltage and 10 nA current. To remove any surface oxide and to get depth profiles of elements of interest, selected areas were sputtered with an ion beam for different durations. Sputtering was accomplished with a 2-kV Xe beam with 1 μA current rastered over a 1 x 1-mm area. The sputtering material removal rate was approximately 160 Å per minute, as measured on an SiO_2/Si standard.

Results and Discussion

Figure 1 shows the secondary electron images for surfaces of HAZ cracks fractured open at the zero-ductility temperature for Heat LP/HS. Morphological features observed at lower magnification (Fig. 1A) indicate a brittle intergranular fracture mode. At higher magnification (Fig. 1B), a view of a single grain facet shows the grain-boundary surface has a textured structure, resembling the skin of an orange. Still higher magnification (20,000X) revealed this textured structure to consist of circular bumps uniformly dispersed on the grain boundary facet — Fig. 2. Very similar observations were made from the comparison heat, Heat HP/LS, whose secondary electron images are shown in Figs. 3 and 4. Formation of bumps (or islands) is characteristic of the Volmer-Weber growth mechanism commonly observed in early stages of thin film formation (Ref. 7).

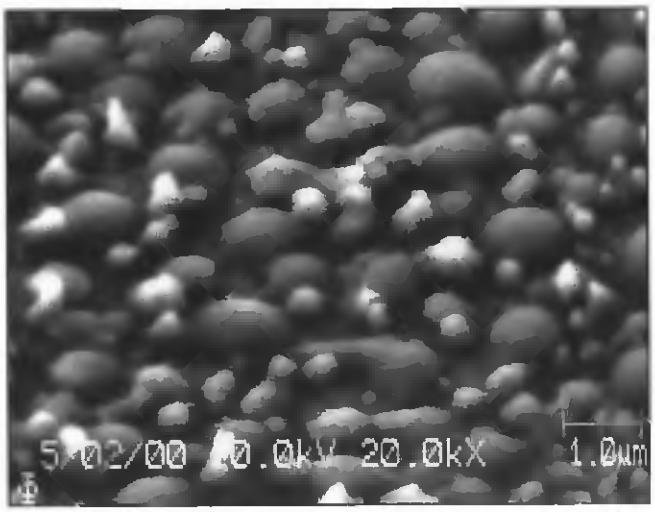

Fig. 2 — SEM image at 20,000X for fractured surface of a HAZ crack formed at the zero-ductility temperature for Heat LP/HS. The textured structure consists of circular bumps uniformly dispersed on the grain boundary facet.

Figures 5 and 6 depict representative Auger survey scans collected from different points in the image (Fig. 2) for the as-tested surface of Heat LP/HS. Specifically, Fig. 5 is from a circular bump feature, while Fig. 6 is from the surrounding matrix. The crack surface is shown to be enriched with O and C, along with S, Si, Na, N, Cl, and K. The Cl, K, and Na detected on the surface undoubtedly resulted from contamination during cutting and handling of the samples because these elements do not exist in the bulk

Table 1 — Chemical Compositions for the Test Material

Heat #	HP/LS	LP/HS
C	0.059	0.060
Mn	1.25	1.26
P	0.027	0.004
S	0.0049	0.032
Si	1.79	1.80
Cr	18.86	19.10
Ni	11.29	11.42
Al	0.004	0.004
Mo	0.010	0.010
Cu	0.010	0.010
N	0.049	0.048
Ni_{eq}	14.34	14.48
Cr_{eq}	18.87	19.11
Cr_{eq}/Ni_{eq}	1.316	1.319

Cr_{eq} and Ni_{eq} used were defined by the WRC-1992 Diagram (Kotecki and Siewert, 1992).

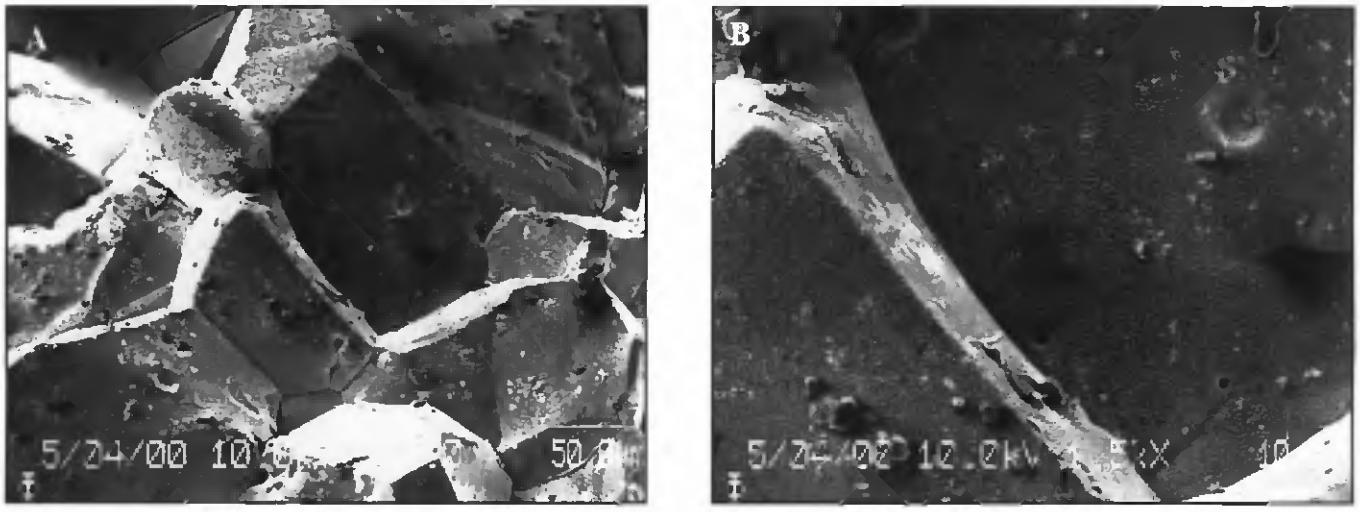

Fig. 3 — The secondary electron images for fractured surfaces of HAZ cracks formed at the ZDT for Heat HP/LS. A — 500X; B — 1500X.

Table 2 — Free Energy of Formation (–ΔG, kJ/mol) Data for Carbides, Phosphides, and Sulfides of Fe, Ni, Cr, Mn, and Si

	Fe	Ni	Cr	Mn	Si
–ΔG	Fe_3C	Ni_3C	Cr_3C_2	Mn_3C_2	SiC
Carbides	4.9	–268	254.3	113.9	53.2
	(1227°C)	(727°C)	(1227°C)	(1227°C)	(1227°C)
–ΔG	FeS	Ni_3S_2	CrS[a]	MnS	
Sulfides	97.3	252	125.6	128.5	
	(727°C)	(227°C)	(727°C)	(1227°C)	
–ΔG	FeO	NiO	Cr_2O_3	MnO	SiO_2
Oxides	197.2	150.7	861.6	312.3	726.9
	(727°C)	(727°C)	(727°C)	(727°C)	(727°C)
–ΔG	Fe_3P	Ni_3P	Cr_3P[b]	MnP_3[c]	
Phosphides	–147.4	–201	123.4	7.33	
	(635°C)	(630°C)	(1427°C)	(951°C)	

Notes:
Unless indicated, most of the data were collected from *Metals Reference Book*, edited by C. J. Smithells, 6th ed., 1983.
(a) Shatynski, S. R. 1977. *Oxid. Met.* 11(6):307.
(b) Zaitsev, A. I., Shelkova, N.E., Litvina, A.D., Mogutnov, B.M., and Dobrokhotova, Zh. V. 1998. Thermodynamic properties and phase equilibria in the Cr-P system, *Journal of the Phase Equilibria* 19(3).
(c) Kubaschewski, O., and Catterall, J.A., 1956. *Thermochemical Data of Alloys*. Pergamon Press, p. 133.

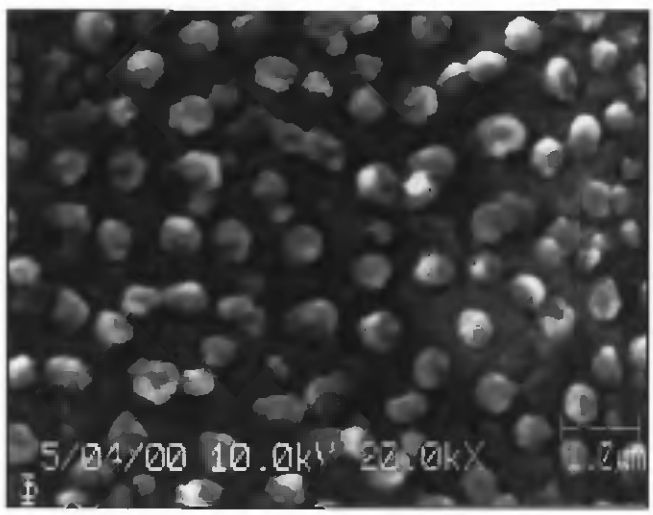

Fig. 4 — SEM image at 20,000X for fractured surface of a HAZ crack formed at the ZDT for Heat HP/LS. The textured structure consists of circular bumps uniformly dispersed on the grain boundary facet.

alloy, and they disappeared after sputtering. The presence of strong O peak indicated the as-tested crack surface was covered with a discontinuous oxide film that most likely developed once the still-hot fractured surfaces were open to the Gleeble chamber atmosphere. Although the tests were conducted under a vacuum of 10^{-3} torr backfilled with argon, there were still possible sources of oxygen, such as from leakage, from traces of oxygen in the argon gas, and from oxygen adsorption in the vacuum chamber. The as-fractured surface did show a slight golden tint, indicating the effect of oxidation. Nevertheless, the much-reduced oxide thickness under the controlled atmosphere made it possible to obtain some useful information through short-time sputtering.

By comparing the spectrum (Fig. 5) from a typical circular bump feature with that from the adjacent "matrix" (Fig. 6), it is apparent the bumps are richer in Si and Cr, and the matrix is richer in Fe. Notice S was detected on the surface at both locations while P was not detected anywhere on the surface, suggesting either it was absent altogether, or its presence was below the detection limit of the Auger system. Chromium peaks were located close to peaks of oxygen, therefore, weak Cr signals were easily buried in the more dominant O peaks. However, careful inspection reveals the less apparent Cr peaks.

After sputtering with Xe ions for 30 s, Auger scans of the same image area for Heat LP/HS exhibited relative changes in peak intensities — Figs. 7 and 8. The most notable changes were the increase of intensity for Fe peaks collected from the matrix adjacent to the circular bumps (Fig. 7) and the increase of intensity for S peaks from both locations. There were still no indications of P being present in the Auger scans. It is apparent removing an approximately 80-Å-thick surface layer by sputtering has begun to reveal the base alloy substrate lying beneath the oxide layer.

The distributions of elements of interest were obtained through mapping. For the area shown in Fig. 2, elemental mappings for Fe, Si, Cr, and S are shown in Figs. 9 through 12, respectively. An analy-

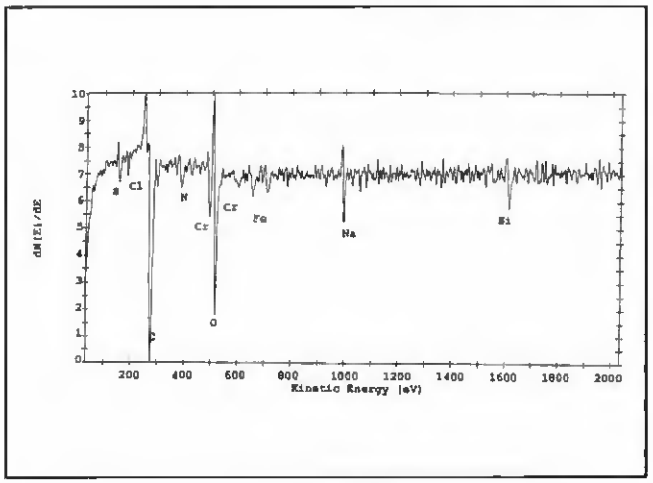

Fig. 5 — A representative Auger survey scan collected from the circular bumps (Fig. 2) for the as-tested surface of Heat LP/HS.

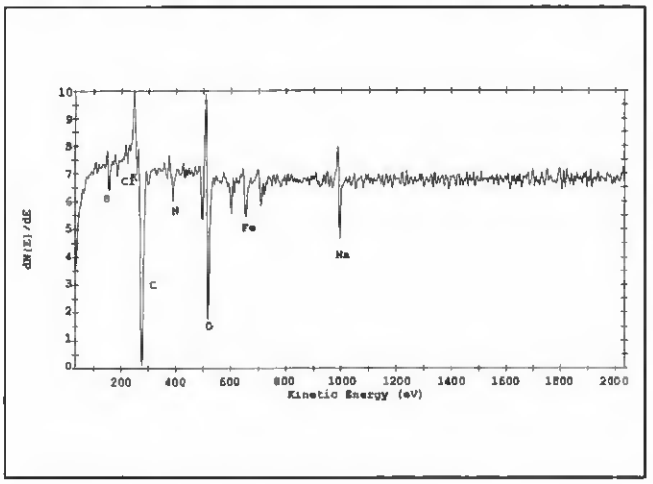

Fig. 6 — A representative Auger survey scan collected from the matrix (Fig. 2) for the as-tested surface of Heat LP/HS.

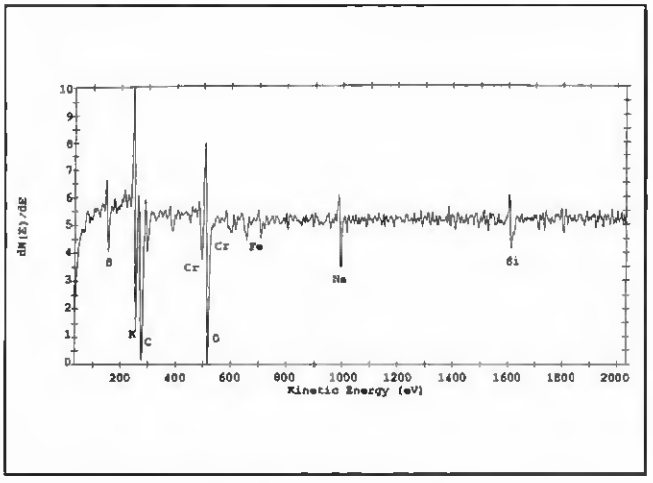

Fig. 7 — A representative Auger survey scan collected from the circular bumps (imaged in Fig. 2) in Heat LP/HS after sputtering with Xe ions for 30 s, removing 80 Å of surface layer.

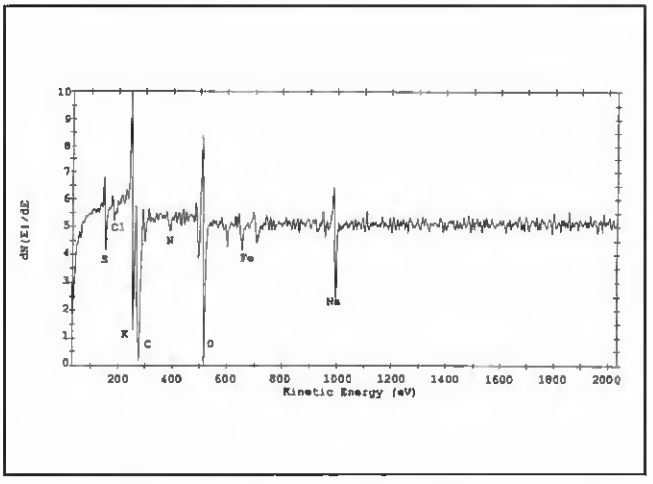

Fig. 8 — A representative Auger survey scan collected from the matrix (imaged in Fig. 2) in Heat LP/HS after sputtering with Xe ions for 30 s, removing 80 Å of surface layer.

sis of elemental distributions reveals Si and Cr are enriched in circular bump features while Fe and S are enriched in the adjacent matrix.

After another 30 s of sputtering by Xe ions (removing a total surface layer approximately 160 Å thick), Auger survey scans from the same image area shown in Fig. 2 were again obtained. Scans from the circular humps (Fig. 13) show decreased intensities for C, disappeared peak for S, and increased intensities for Si, Cr, and Fe. Scans from the matrix (Fig. 14) depict much-increased Fe and Cr peaks along with a decreased peak for O; most other elements, including S, disappeared from the spectrum.

For the comparison heat, Heat HP/LS, the initial Auger survey scans of the as-fractured surface showed the spec-

Table 3 — Diffusivity of P, S, C, Cr, and Mn Ferrite and Austenite Near 1200 °C

	A(cm²/s)	Q (kcal/mol)	D (cm²/s)
P in ferrite (1300°C)	2.9	54.9	6.61×10^{-8}
P in austenite (1300°C)	28.3	69.8	5.66×10^{-9}
S in ferrite (1300 °C)	1.35	48.4	5.66×10^{-8}
S in austenite (1300°C)	2.42	53.4	9.2×10^{-8}
C in austenite (1200°C)	0.668	37.46	1.85×10^{-6}
Cr in austenite (1200°C)	0.0012	55.2	2.16×10^{-11}
Si in austenite (1293°C)	—	—	1.7×10^{-9}
Mn in austenite	0.57	66.2	8.57×10^{-11}

Note:
Data for chemical diffusion (A and Q) were collected from *Metals Reference Book*, edited by C. J. Smithells, 5th Ed., 1976. Arrhenius equation, $D = A \cdot \exp(-Q/RT)$, was used for calculating D from A and Q.

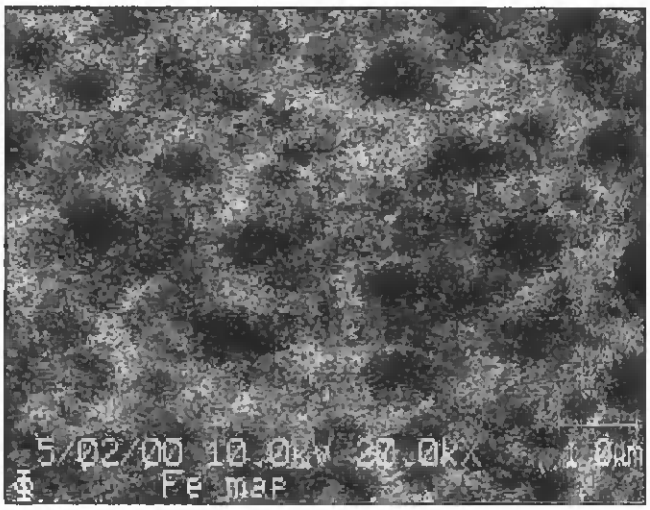

Fig. 9 — Distribution of Fe in the area shown in Fig. 2 after sputtering for 30 s.

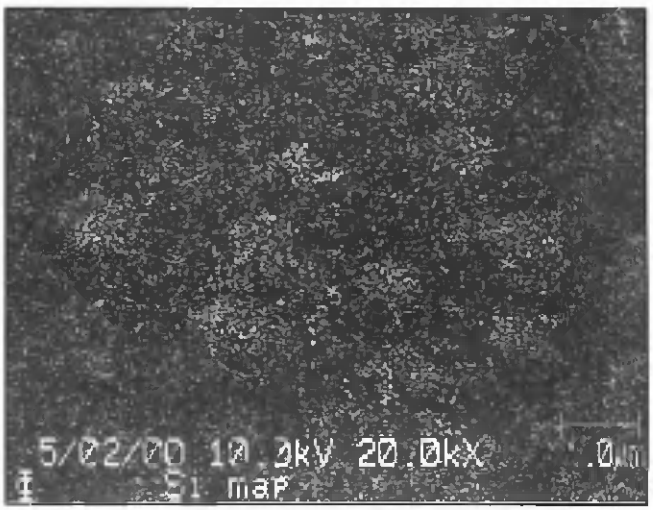

Fig. 10 — Distribution of Si in the area shown in Fig. 2 after sputtering for 30 s.

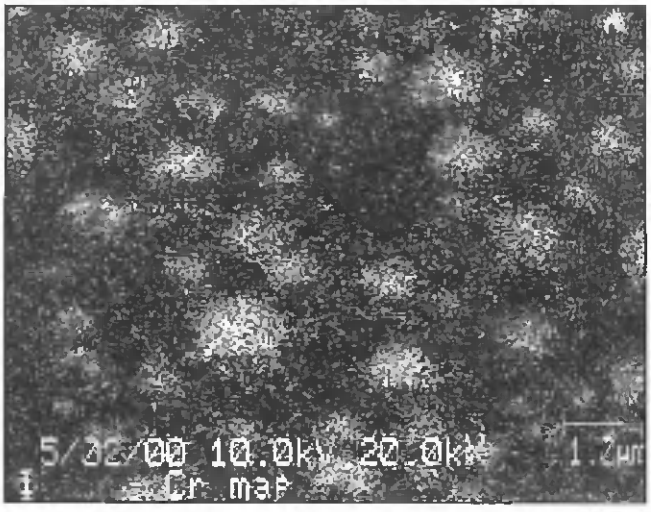

Fig. 11 — Distribution of Cr in the area shown in Fig. 2 after sputtering for 30 s.

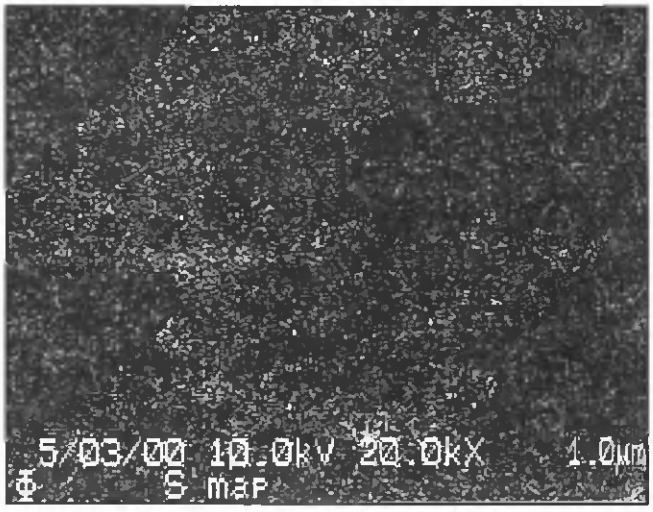

Fig. 12 — Distribution of S in the area shown in Fig. 2 after sputtering for 30 s.

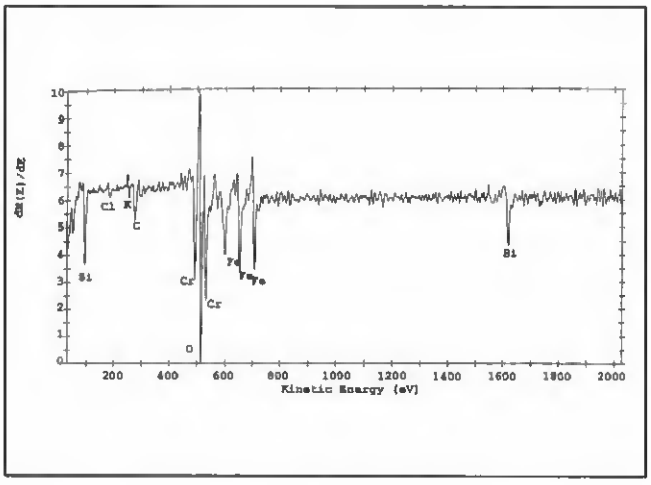

Fig. 13 — A representative Auger survey scan collected from the circular bumps (imaged in Fig. 2) in Heat LP/HS after sputtering with Xe ions for 60 s, removing the 160-Å surface layer.

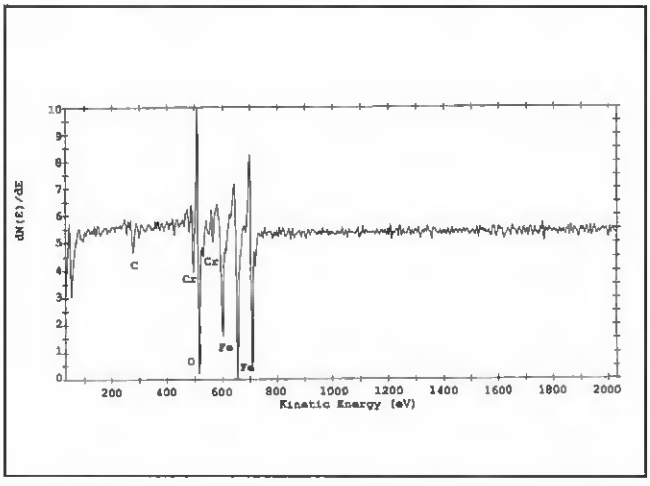

Fig. 14 — A representative Auger survey scan collected from the matrix (imaged in Fig. 2) in Heat LP/HS after sputtering with Xe ions for 60 s, removing 160 Å surface layer.

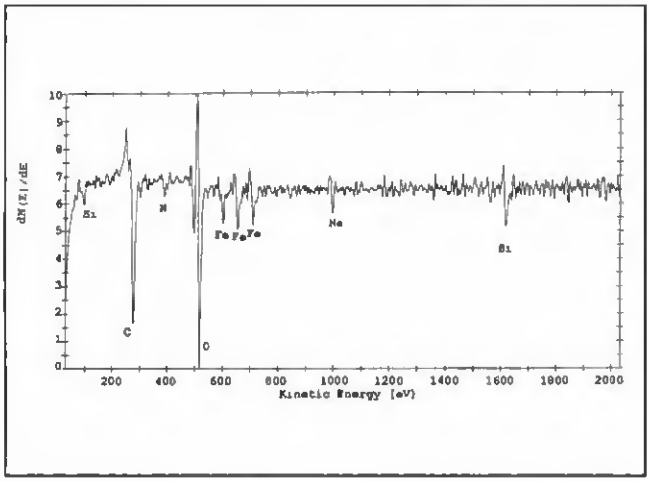

Fig. 15 — A representative Auger survey scan collected from the circular bumps (Fig. 4) for the as-tested surface of Heat HP/LS.

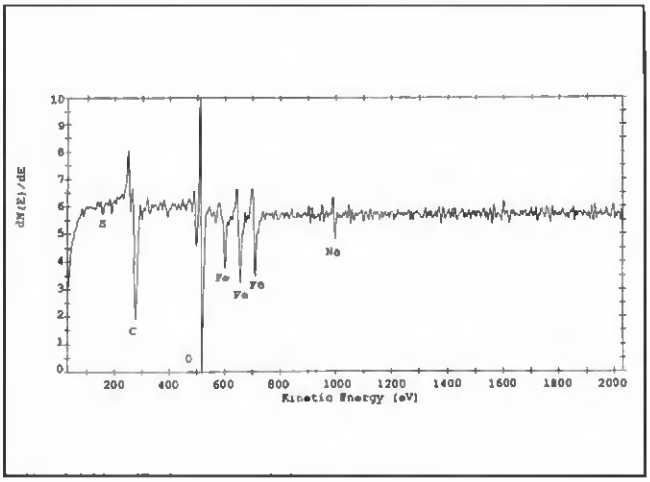

Fig. 16 — A representative Auger survey scan collected from the matrix (Fig. 4) for the as-tested surface of Heat HP/LS.

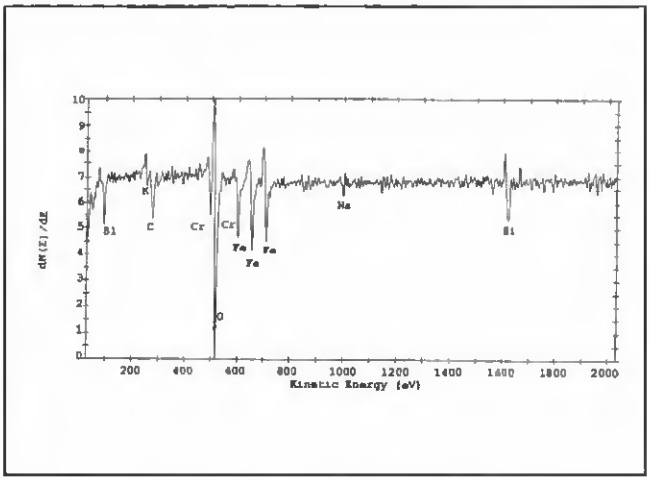

Fig. 17 — A representative Auger survey collected from the circular bumps (imaged in Fig. 4) in Heat HP/LS after sputtering with Xe for 12 s.

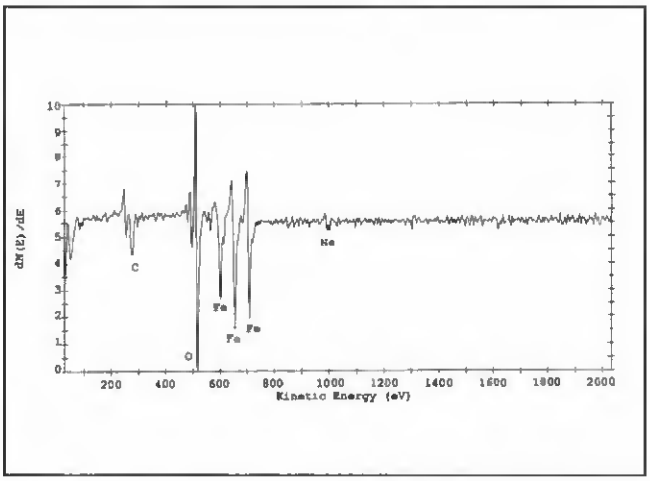

Fig. 18 — A representative Auger survey collected from the matrix (imaged in Fig. 4) in Heat HP/LS after sputtering with Xe for 12 s.

trum from the circular bumps was rich with O and C, with some Si, Fe, and Na also present — Fig. 15. Spectrum from the adjacent matrix does not show the Si peaks — Fig. 16. No P or S peaks appeared on the spectrums from these Auger survey scans of as-tested crack surfaces. After sputtering with Xe ions for 12 s (removing an approximately 30-Å- thick surface layer), the spectrum from the circular bumps (Fig. 17) shows the intensities of Si and Fe peaks have increased, while the intensity of C peak has decreased. The spectrum from the matrix (Fig. 18) shows a similar trend, indicating the removal of surface contaminants (*e.g.*, Na and C) and revealing of substrate elements (*e.g.*, Fe). This trend continued after sputtering for another 30 s (removing a total of approximately 110-Å-thick surface layer). At this point, a Ni peak started to be detected, indicative of the substrate — Figs. 19 and 20.

Although Heat HP/LS contains a high level of P and low level of S, the P peak in spectra from both as-fractured and sputtered surfaces was too low to positively identify it with the equipment employed. However, the presence of S was detected on the surface, especially in the matrix areas. This result strongly supported the contention that S diffuses faster and segregates more severely than P in the HAZ. It is clear exposure of fractured surfaces to the Gleeble chamber atmosphere produced oxide films with a relative tendency of formation that can be predicted according to the ranking of free energies of formation of oxides. The free energies of oxide formation for major alloying elements involved are listed in Table 2.

In the on-cooling temperature range following fracture around 1300°C, Cr_2O_3 and SiO_2 have the greatest negative free energies of formation, meaning Cr and Si have the strongest tendency to oxidize. The actual rate for oxidation is affected by the diffusion rates for the species involved. Diffusivity data available from the literature were compiled for temperatures at or near 1300°C (Table 3). It can be seen the diffusivity for Si in the temperature range is almost as high as that for S, being two orders of magnitude higher than both Cr and Mn. As a result, Si alone seems to be the most kinetically favorable candidate to migrate to the surface for oxidation during rapid cooling.

Recall that with partial removal of surface oxide films by sputtering, S concen-

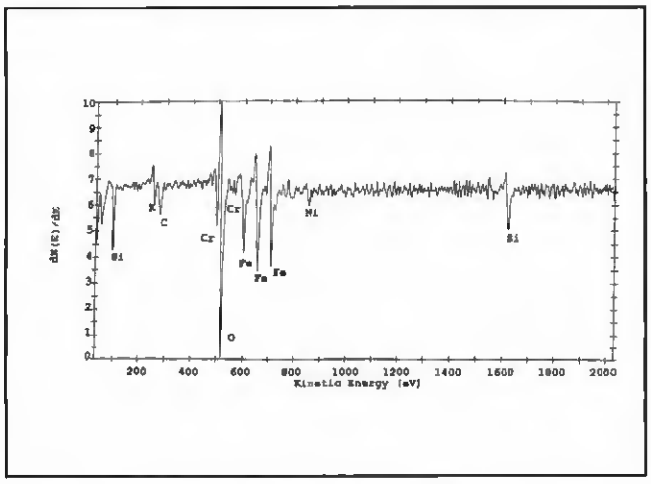

Fig. 19 — A representative Auger survey scan collected from the circular bumps (imaged in Fig. 4) in Heat HP/LS after sputtering for 42 s, removing the 110-Å surface layer.

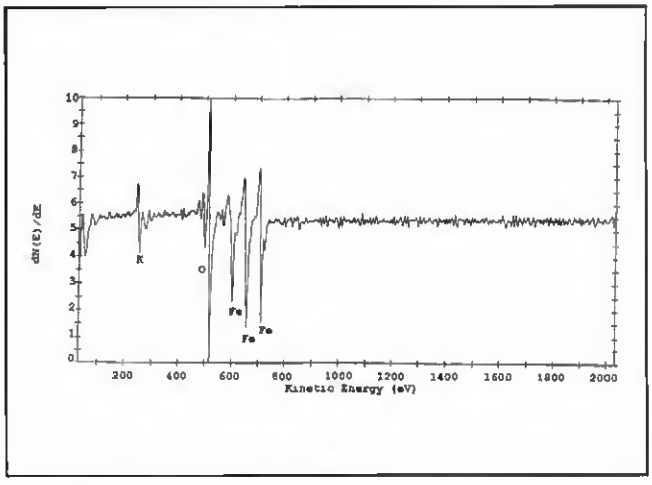

Fig. 20 — A representative Auger survey scan collected from the matrix (imaged in Fig. 4) in Heat HP/LS after sputtering for 42 s, removing the 110- Å surface layer.

tration showed a maximum level just below the surface. This result may be explained by reconstructing a possible sequence of reactions on the fracture surface. It is reasonable to believe that at the moment of fracture, S had segregated to the grain boundaries while slower P had not. Although Si is not a strong grain boundary segregate in austenitic stainless steels (Ref. 7), the exposure to oxidizing atmosphere seems to have provided the driving force for Si to rapidly migrate to the surface and to preferentially form Si-rich oxide. It appears that for HAZ hot cracking, S is a faster diffuser and tends to segregate to the grain boundaries more than P. Following cracking and while still at high temperature, crack surfaces have been covered by an oxide film enriched with Si. Such artifacts may be avoided if sample preparation procedures can be refined to prevent any exposure to an oxidizing atmosphere during handling. But this is very difficult.

Conclusions

From the Auger analysis of simulated HAZ hot crack surfaces in Type 308 austenitic stainless steel, the following conclusions can be drawn.

Sulfur strongly segregates to the intergranular fracture surface, while segregation of P was undetected by the Auger equipment employed. Such segregation behavior correlated well with the cracking susceptibility results (Ref. 1) that showed S to be more detrimental than P to HAZ cracking. The observed segregation behavior seems to support the assumptions that in the heat-affected zone, S is a faster diffuser and tends to segregate to the grain boundaries more than P, while P is a slow diffuser and segregates less severely than S. Following cracking and while still at high temperature, the crack surface is covered by an oxide film enriched with Si, even in the controlled chamber atmosphere employed in this study. The preference for formation of Si-rich oxide is supported by thermodynamic and diffusivity data in the temperature range for the HAZ.

Acknowledgments

This study was funded by the High Alloys Committee of the Welding Research Council of New York, N.Y. Dr. A. Linsebigler and M. Burrell of General Electric Research and Development Center in Schenectady, N.Y., provided valuable help in conducting the Auger analysis. Dr. W. Chen of Dynamic Systems, Inc., allowed us to use their latest Gleeble machines.

References

1. Li, L., and Messler, R. W., Jr. 1999. The effect of phosphorus and sulfur on susceptibility to weld hot cracking in austenitic stainless steels. *Welding Journal* 78(12): 387-s to 396-s.

2. Brooks, J. A. 1975. Weldability of high N, high Mn austenitic stainless steel. *Welding Journal* 54(6): 189-s to 195-s.

3. Arata, Y., Matsuda, F., and Katayama, S. 1977. Solidification crack susceptibility in weld metals of fully austenitic stainless steels (Report II). *Transactions of JWRI* 6(1): 105.

4. Arata, Y., Matsuda, F., Nakagawa, H., and Katayama, S. 1978. Solidification crack susceptibility in weld metals of fully austenitic stainless steels (Report IV). *Transactions of JWRI* 7(2): 21.

5. Barkleit, G., John, A., and Schneider, F. 1999. Scanning AES and chemical investigation of materials failure due to phosphorus and sulphur grain boundary segregation in Type 304L stainless steel. *Materials and Corrosion* 50(10): 591.

6. Nippes, E. F., and Savage, W. F., 1949. Tests of specimens simulating weld heat-affected zone. *Welding Journal* 28(12): 599-s.

7. Feldman, L. C., and Mayer, J. W., 1986. *Fundamentals of Surface and Thin Film Analysis*, pp. 136–141. New York: North Holland-Elsevier.

8. Li, L. 2000. Effects of composition and microstructure on constitutional liquation in a Nb-bearing austenitic stainless steel. Ph.D. dissertation, Rensselaer Polytechnic Institute, Troy, N.Y.